SCIENCE CHINA
Chemistry

• ARTICLES •

February 2018 Vol.61 No.2: 164–171
https://doi.org/10.1007/s11426-017-9099-6

Synthesis of novel magnetic sulfur-doped Fe_3O_4 nanoparticles for efficient removal of Pb(II)

Xueqiong Huang†, Long Kong†, Shouqiang Huang, Min Liu & Liang Li*

School of Environmental Science and Engineering, Shanghai Jiao Tong University, Shanghai 200240, China

Received May 3, 2017; accepted June 14, 2017; published online September 15, 2017

In this work, we report the synthesis of magnetic sulfur-doped Fe_3O_4 nanoparticles (Fe_3O_4:S NPs) with a novel simple strategy, which includes low temperature multicomponent mixing and high temperature sintering. The prepared Fe_3O_4:S NPs exhibit a much better adsorption performance towards Pb(II) than bare Fe_3O_4 nanoparticles. FTIR, XPS, and XRD analyses suggested that the removal mechanisms of Pb(II) by Fe_3O_4:S NPs were associated with the process of precipitation (formation of PbS), hydrolysis, and surface adsorption. The kinetic studies showed that the adsorption data were described well by a pseudo second-order kinetic model, and the adsorption isotherms could be presented by Freundlich isotherm model. Moreover, the adsorption was not significantly affected by the coexisting ions, and the adsorbent could be easily separated from water by an external magnetic field after Pb(II) adsorption. Thus, Fe_3O_4:S NPs are supposed to be a good adsorbents for Pb(II) ions in environmental remediation.

sulfur-doped Fe_3O_4 nanoparticles, Pb(II) adsorption, magnetic separation

Citation: Huang X, Kong L, Huang S, Liu M, Li L. Synthesis of novel magnetic sulfur-doped Fe_3O_4 nanoparticles for efficient removal of Pb(II) . *Sci China Chem*, 2018, 61: 164–171, https://doi.org/10.1007/s11426-017-9099-6

1 Introduction

In recent years, magnetic ferrite nanoparticles have been extensively exploited as one of the most promising nanomaterials because of their advantages of nano-size, large specific surface area, easy separation, and environmental friendliness [1–8]. Among various applications, the removal of target contaminants from wastewater by magnetic ferrite nanoparticles (particularly Fe_3O_4) has caught great attention [9–20]. Wang *et al.* [11] used water-soluble Fe_3O_4 nanoparticles (Fe_3O_4 NPs) as adsorbents for heavy metals in wastewater, which exhibited a higher adsorption capacity for Pb(II) and Cr(VI) than water-insoluble Fe_3O_4 NPs. In order to improve the adsorption performance of Fe_3O_4 NPs, various surface modifications have been employed, and the modified nanoparticles show more effective removal of heavy metals [12–14]. Due to the high affinity of –SH groups to heavy metal ions based on Lewis acid-base interactions between sulfur atoms and metal ions [15,16], thiolation for Fe_3O_4 NPs has attracted much concern. Yantasee *et al.* [17] utilized *m*-2,3,dimercaptosuccinic acid (DMSA) to functionalize Fe_3O_4, and the composite could be an efficient adsorbent for heavy metals (Pb, As, Hg, Cd, and Tl) in water and human blood and plasma. Mercaptopropyl-triethoxysilane (MPTES) [18], ethanedithiol (EDT) [19], and poly (acrylic acid)-hydroxyethyl disulfide (PAA-HED) [20] have also been employed to functionalize Fe_3O_4 NPs, while the resultant adsorption capacities are not so satisfactory. On the other hand, researchers are paying great attention to the elements doping to improve adsorption properties of Fe_3O_4 magnetic nanomaterials, such as Mn, Cu, V, Ni, Zn, Ba, Cd, Sr, Ti [21–24]. On the basis of aforementioned statements, it is

†These authors contributed equally to this work.
*Corresponding author (email: liangli117@sjtu.edu.cn)

expected that the Fe_3O_4 NPs might have a better adsorption performance by combining the role of sulfur (S) in the adsorption process with the modifying function of doping strategy. To the best of our knowledge, there are quite few reports on the research of S-doped Fe_3O_4 NPs, and their applications for the removal of heavy metals.

In the present work, sulfur-doped Fe_3O_4 NPs (Fe_3O_4:S NPs) with excellent sorption performance and easy magnetic separation were first prepared using a simple mixing and sintering method. The nanoparticles were characterized by X-ray diffraction (XRD), transmission electron microscope (TEM), energy dispersive X-ray fluorescence (ED-XRF), Fourier transform infrared (FTIR), and vibrating sample magnetometer (VSM) analyses. Then we investigated the adsorption properties of the prepared nanoparticles for Pb(II) in the aqueous solution, including the effects of the initial pH and coexisting ions. Furthermore, the kinetic adsorption process and the adsorption isotherms were studied. It is notable that the Fe_3O_4:S NPs exhibit a more effective adsorption performance than bare Fe_3O_4 NPs. Finally, the corresponding mechanisms for Pb(II) removal were discussed.

2 Experimental

2.1 Materials

Iron (III) nitrate nonahydrate ($Fe(NO_3)_3·9H_2O$, 98.5%), thiourea (≥99.0%), 1-butylamine (≥99.5%), and lead nitrate (99%) were provided by Aladdin Chemical (Shanghai, China). All chemicals were used without any further purification in the experiments. Distilled water (DI) (>18 MΩ cm) was used for preparing the Pb(II) solution.

2.2 Synthesis of Fe_3O_4:S NPs

The synthesis method was similar to that previously used for $CuInS_2$ nanocrystals preparation [25]. In a typical procedure, solution A and B were prepared by dissolving 30 mmol of thiourea and 10 mmol of $Fe(NO_3)_3$ into 50 mL 1-butylamine with two separate beakers, separately. After ultrasonic dispersion, the two solutions were mixed in a 250 mL three-neck flask under stirring. The resulting mixture was heated to 60 °C and then kept stirring for 2 h in the atmosphere of flowing nitrogen. After cooling to room temperature, the dark brown colored mixture was washed with methanol and acetone for several times and dried in a vacuum oven for 1 h at 60 °C. Then the product was sintered at 300 °C for 2 h, which were labeled as Fe_3O_4:S. For comparison, the same experimental procedure was used for the synthesis of bare Fe_3O_4 NPs without the addition of thiourea.

2.3 Characterization

The XRD measurement was recorded on a Shimadzu XRD-6100 (Japan). Morphologies of the samples were characterized using a TEM (JEM-2100F operating at 200 kV, Japan). The ED-XRF (EDX-720) analysis was conducted to determine the concentration of Fe, O, and S. FTIR spectra were collected by using a Thermo Nicolet 6700 spectrometer (USA) over the wavelength range of 4000–400 cm^{-1}, using KBr as a reference. The magnetic measurement was carried out on a PPMS-9T (EC-II) of Quantum Design with a magnetic field up to 3 T. X-ray photoelectron spectroscopy (XPS) analysis was performed on a Thermo Scientific Escalab 250Xi Photoelectron Spectrometer (USA) with a monochromatic Al Kα radiation source.

2.4 Adsorption experiments

To determine the optimum pH for Pb(II) adsorption experiments, the influence of solution pH on adsorption was examined first. 0.1 M HCl and NaOH were utilized to adjust the initial pH of the solutions from 2.0–6.0. The adsorbent (20 mg) was added to 40 mL of Pb(II) solution (100 mg L^{-1}) under continuous stirring at 30 °C for 24 h. Then the optimum pH was obtained.

Adsorption experiments were carried out by mixing adsorbents and the Pb(II) solutions with different concentrations under continuous stirring (30 °C). At certain intervals, the solutions were collected and filtered through a 0.22 μm membrane to determine the concentration of Pb(II). From the obtained results, adsorption kinetic and adsorption isotherm were studied.

To test the influence of competing ions, 30 mg of adsorbent was added to 50 mL of Pb(II) solution (100 mg L^{-1}) containing competing ions of Ca(II), Mg(II), Zn(II), Cd(II), or Cu(II) under continuous stirring (30 °C, 24 h). The concentrations of the competing ions were set at 0.48 and 0.96 mM to control the molar ratios of competing ions to Pb(II) at 1 and 2, respectively. Moreover, a control test was conducted under the same conditions in the absence of competing ions.

The concentration of Pb(II) and total iron in the filtrates was analyzed using an atomic adsorption spectrometer (ControlAA 700, Analytik Jena AG, Germany). The adsorbent after adsorption was separated from the solution by high-speed centrifuge, and then dried in a vacuum oven (60 °C) to identify the removal mechanisms.

3 Results and discussion

3.1 Characterization

Figure 1 shows the XRD patterns of the prepared samples. The diffraction peaks at 30.10°, 35.42°, 43.05°, 56.94°, and 62.52° matched well with the (220), (311), (400), (511), and (440) planes of magnetite Fe_3O_4 (JCPDS Card No. 19-0629), respectively, which proved that the well crystallized Fe_3O_4 NPs were prepared successfully under 300 °C. As for

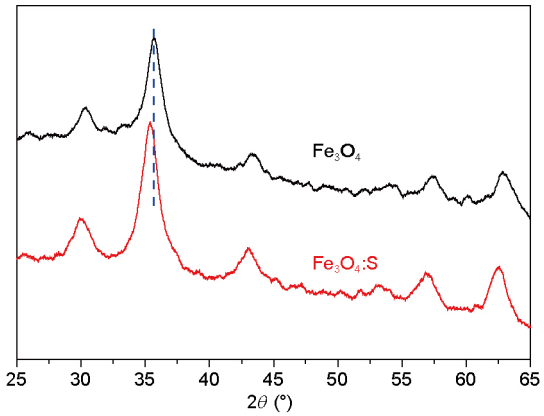

Figure 1 XRD patterns of the prepared samples (color online).

Fe_3O_4:S, it is worth noting that its characteristic peaks have shifted to smaller angles in comparison with those of Fe_3O_4, which may be originated from the sulfur doping [26,27].

The morphology of Fe_3O_4:S and Fe_3O_4 are illustrated in Figure 2. It is found that the prepared Fe_3O_4:S and Fe_3O_4 were well crystallized, and the Fe_3O_4:S NPs have a size ranging from 3 to 6 nm with an average size of 4.39 nm. The clear lattice fringes with a d-spacing of 0.243 nm are assigned to the (222) planes of Fe_3O_4 (Figure 2(b)). Comparably, the Fe_3O_4 NPs exhibited a larger sizes (ranging from 8 to 13 nm with an average size of 10.46 nm) with a (222) lattice plane of 0.244 nm. These results further indicate that the well-crystallized Fe_3O_4 NPs remained under 300 °C after the introduction of S. Furthermore, as illustrated in Table 1, the Fe_3O_4:S nanoparticles contained O, Fe, S and other trace elements, the S content was 7.54 wt%, which proved that S had been doped into Fe_3O_4 NPs.

Figure 3 presents the FTIR spectra of Fe_3O_4 and Fe_3O_4:S, Fe–O bond appeared at 567 cm^{-1} in both spectra [28]. It can be seen that the introduction of S will not obviously change the structural and functional properties of Fe_3O_4 except for two new peaks appearing at 1016 and 977 cm^{-1}, which could be assigned to C–O bond [29,30].

The magnetic properties of Fe_3O_4:S and Fe_3O_4 are depicted in Figure 4. Fe_3O_4:S exhibited superparamagnetic behavior at 300 K with no obvious hysteresis and coercivity. On the basis of the physical property measurement system at 3 T, the saturation magnetization of Fe_3O_4:S and Fe_3O_4 were 32.97 and 37.43 emu g^{-1}, respectively. The lower saturation magnetization of Fe_3O_4:S may be attributed to the introduction of S or the smaller particle size of Fe_3O_4:S. While the magnetic intensity was enough for the efficient magnetic separation. It had been confirmed that Fe_3O_4:S could be easily dispersed in aqueous solution and separated from their dispersion by a permanent magnet (inset of Figure 4).

3.2 Effect of pH on Pb(II) adsorption

The effect of initial pH on Pb(II) removal was investigated at the pH range of 2.0–6.0 due to the possibility of Pb(II) hydroxide precipitation at the pH higher than 6.0 [31], the results were shown in Figure 5. The Pb(II) adsorption yield increased markedly from 11.87 to 102.95 mg g^{-1} when increasing the pH. H^+ and Pb(II) are both positively charged, which may lead to the occurrence of competitive adsorption, so that the metal ions can be more effectively adsorbed at high pH [32]. Within the investigated pH range, the Fe release amount of Fe_3O_4:S was about 4.01–18.07 mg L^{-1}, which was higher than that of Fe_3O_4, but much lower than iron sulfides [31]. Given the pH-dependent sorption behavior of Fe_3O_4:S NPs, here we chose the pH 6.0 for further sorption studies.

3.3 Adsorption kinetics

The adsorption kinetics of Pb(II) on the synthesized adsorbents as a function of the contact time are shown in Figure 6(a). The plots represent the amount of Pb(II) adsorbed by the sorbent (q_t) versus contact time (t). It was noteworthy that the adsorption of Pb(II) by Fe_3O_4:S NPs was rapidly proceeded during the first 30 min, and then it reached equilibrium after 120 min with a superior adsorption capacity. Meanwhile, the Fe release amount increased over time, and didn't show the decline trend observed in previous report (Figure 6(b)) [33]. Comparatively, the adsorption capacity of Fe_3O_4 NPs was much lower. Therefore, the addition of S is vital to the adsorption performance.

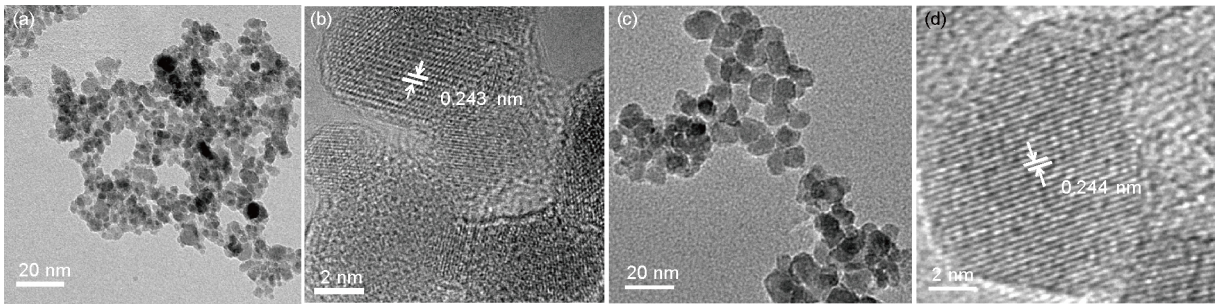

Figure 2 TEM images of the prepared nanoparticles. (a) TEM image of Fe_3O_4:S; (b) high-resolution TEM (HR-TEM) image of Fe_3O_4:S; (c) TEM image of Fe_3O_4; (d) HR-TEM image of Fe_3O_4.

Table 1 Weight percentage of major components of Fe_3O_4:S and Fe_3O_4

Sample	O	Fe	S	Others
Fe_3O_4:S	24.80	67.50	7.54	0.16
Fe_3O_4	26.38	73.23	0.01	0.38

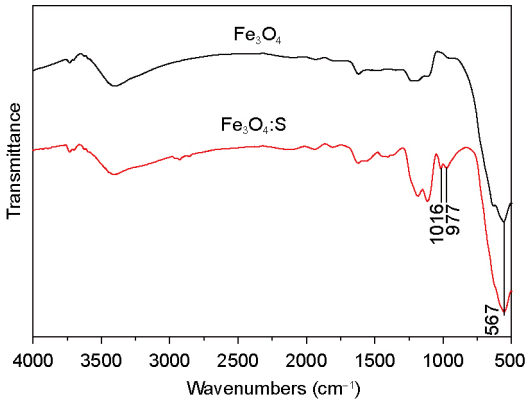

Figure 3 FTIR spectra of Fe_3O_4 and Fe_3O_4:S (color online).

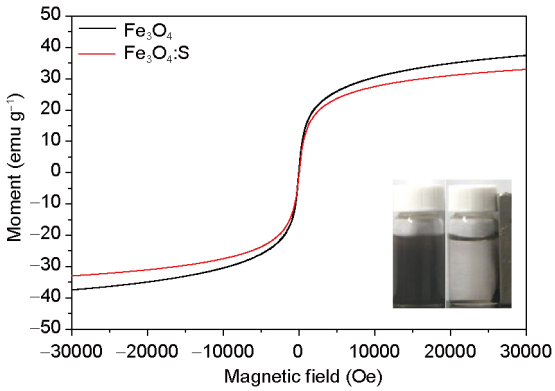

Figure 4 Magnetization curves of Fe_3O_4:S and Fe_3O_4. Inset are the photographs of dispersion of Fe_3O_4:S in aqueous solution (left) and its response to a magnet (right) (color online).

In order to investigate the adsorption process on Fe_3O_4:S NPs, two different kinetic models, the pseudo-first-order model and pseudo-second-order model, were applied to analyze the kinetic data. The equations can be expressed as follows [31,34]:

$$\ln(q_e - q_t) = \ln q_e - k_1 t \quad (1)$$

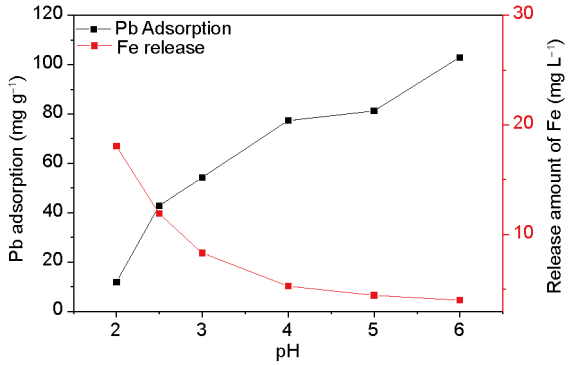

Figure 5 The influence of initial pH on the adsorption of Pb(II) and Fe release of Fe_3O_4:S NPs. Experimental conditions: initial Pb(II) concentration is 100 mg L^{-1} (40 mL), sorbent dosage is 20 mg, pH 2.0–6.0, contact time is 24 h, temperature is 30 °C (color online).

$$\frac{t}{q_t} = \frac{1}{k_2 q_e^2} + \frac{1}{q_e} t \quad (2)$$

where q_e and q_t refer to the amount of sorption at any time t and equilibrium (mg g^{-1}), respectively. k_1 (min^{-1}) and k_2 (g mg^{-1} min^{-1}) are the rate constants of the two kinetic models. From the two models, the adsorption parameters and correlation coefficients (R^2) were obtained and given in Table 2. The plot of t/q versus t shows better linearity in the pseudo-second-order model (Figure 6(b)), and the adsorption capacity calculated from this model was close to the experimental values, which suggested that chemical reactions were significant present in the rate-controlling step [35]. In this study, it meant that chemisorption played an important role in the adsorption process of Pb(II) on Fe_3O_4:S NPs.

3.4 Adsorption isotherm

To explore the adsorption performance more in-depth, the adsorption isotherm of Pb(II) on Fe_3O_4:S NPs was performed. As shown in Figure 7(a), q_e increased with a raise in equilibrium concentration (C_e). Two typical adsorption models, the Langmuir and Freundlich models, were used to simulate the sorption isotherms of Pb(II). The most common sorption model used to fit the experimental data is Langmuir isotherm [36]:

$$\frac{C_e}{q_e} = \frac{C_e}{q_m} + \frac{1}{q_m K_L} \quad (3)$$

Table 2 Parameters associated with kinetic models for the adsorption of Pb(II)

	The rate constant	q_e (mg g^{-1})	R^2
pseudo-first-order model	$k_1 \times 10^{-2}$ (min^{-1}) 0.50	38.28	0.940
pseudo-second-order model	$k_1 \times 10^{-4}$ (g mg^{-1} min^{-1}) 5.48	90.91	0.999

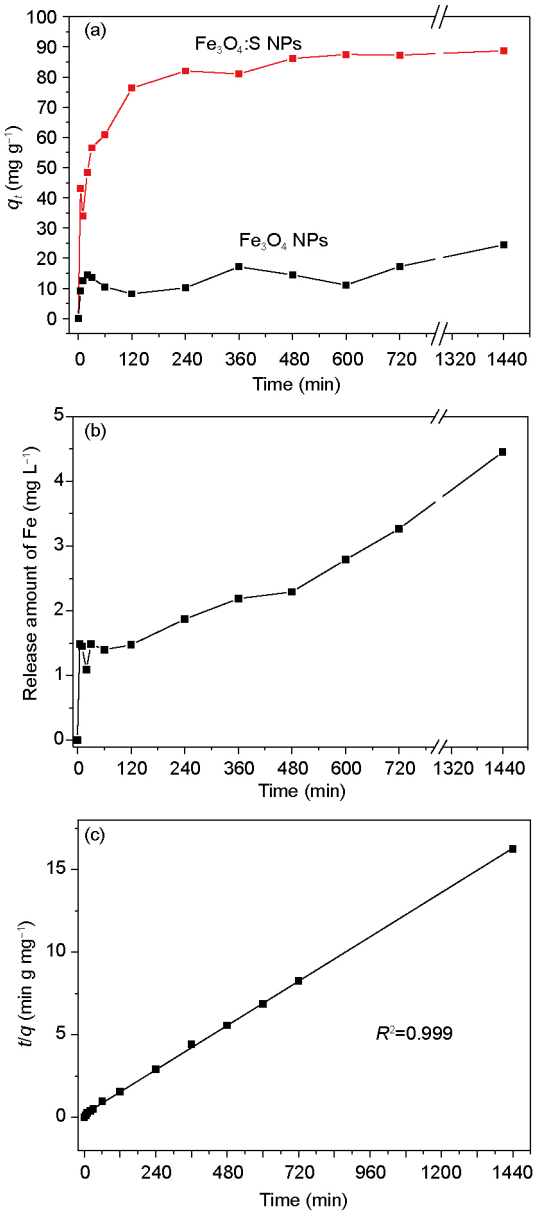

Figure 6 (a) Adsorption kinetics of Pb(II) on Fe_3O_4:S NPs and Fe_3O_4 NPs; (b) Fe releasing kinetics of Fe_3O_4:S NPs; (c) the pseudo-second-order model for adsorption of Pb(II) on Fe_3O_4:S NPs. The symbols indicate experimental data and the solid lines represent the fitted curves. Experimental conditions: initial Pb(II) concentration is 100 mg L^{-1} (100 mL), sorbent dosage is 60 mg, pH 6.0, contact time is 24 h, temperature is 30 °C (color online).

where q_e is the adsorption amount of Pb(II) on sorbents (mg g^{-1}), C_e is the Pb(II) equilibrium concentration in solution (mg L^{-1}), q_m and K_L represent the maximum adsorption capacity of Pb(II) and the energy constant related to the heat of adsorption, respectively. The model is valid for monolayer sorption on surfaces containing a finite number of identical sorption sites.

Freundlich isotherm is an empirical equation, which is shown to be consistent with exponential distribution of active centers, and it can be indicated that the adsorption process of

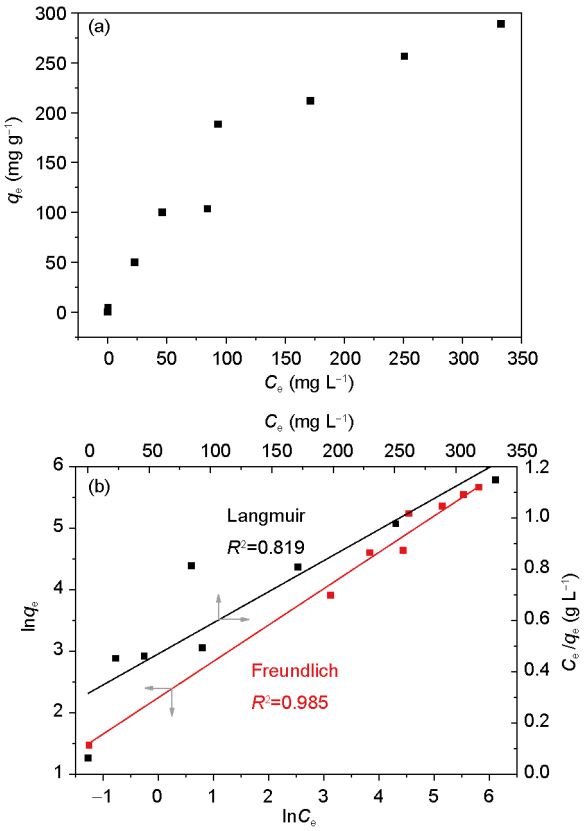

Figure 7 (a) Adsorption isotherm of Pb(II) on Fe_3O_4:S NPs; (b) the fitting of Langmuir and Freundlich models, symbols are experimental data, solid lines represent the fitted curves. Experimental conditions: initial concentration is 5–500 mg L^{-1} (40 mL), sorbent dosage is 20 mg, pH 6.0, contact time is 24 h, temperature is 30 °C.

metal ions mainly occurs on a heterogeneous surface [37]. The formula of the Freundlich isotherm can be expressed as [38]:

$$\ln q_e = \ln K_F + \frac{1}{n}\ln C_e \quad (4)$$

where K_F is the maximum adsorption capacity, and $1/n$ refers to the Freundlich adsorption intensity parameter, q_e and C_e have the same meaning as Eq. (3) does. The fitting plots based on the two isotherm models are shown in Figure 7(b).

It can be seen that the adsorption of Pb(II) on Fe_3O_4:S NPs was better estimated by the Freundlich model with a higher correlation coefficient (R^2) of 0.985, implying that the adsorption process is mainly attributed to the heterogeneous adsorption [37]. The maximum adsorption capacity (q_m) calculated from the Langmuir model was 500 mg g^{-1}, and K_L was found to be 0.00653 L mg^{-1}. The value of $1/n$ obtained from the Freundlich isotherm was 0.604, which was less than 1.0, indicating a favorable adsorption condition [37]. A comparison of the maximum adsorption capacity of Pb(II) among Fe_3O_4:S NPs and other adsorbents were given in Table 3.

Table 3 Comparison of Langmuir sorption capacity (q_m) for the sorption of Pb(II) by adsorbents

Sorbent	q_m (mg g^{-1})	Ref.
β-cyclodextrin stabilized nano-Fe_3S_4	256	[35]
synthetic iron sulphide	33.27	[34]
thiol-functionalized magnetic mesoporous silica	91.50	[39]
thiol-functionalized multiwall carbon nanotube/Fe_3O_4	65.40	[20]
multiwall carbon nanotubes/Fe_3O_4	41.77	[13]
water-soluble Fe_3O_4 nanoparticles	96.80	[12]
sulfur-doped Fe_3O_4 nanoparticles	500	This work

3.5 Effect of competing ions

The effects of ions (Cd(II), Cu(II), Zn(II), Mg(II), and Ca(II)) on Pb(II) removal by Fe_3O_4:S NPs were studied, since they were expected to exist in natural water, and always had influences on the adsorption of metal ions. The results showed in Figure 8 indicate that Mg(II) ion has no obvious effect on the adsorption capacity, while the addition of the other four ions decreased the adsorption capacity to a certain degree. The influence sequence of the five competing ions is Cu(II)≈Zn(II)>Cd(II)>Ca(II)>Mg(II).

3.6 Removal mechanisms

FTIR spectra of Fe_3O_4:S NPs before and after Pb(II) adsorption are presented in Figure 9. It can be seen that the peak of hydroxyl compounds at 3405 cm^{-1} exhibited some changes, and the peaks at 1625, 1112, 977, and 553 cm^{-1} showed minor shift to 1627, 1122, 971, and 588 cm^{-1}, respectively. The C–O group at 1016 and 1187 cm^{-1} [30,40] sharply decreased after adsorption, which may be attributed to the involvement of these groups in the adsorption process. In addition, there is a new peak appearing at 1384 cm^{-1}, which corresponded to the strain mode of NO_3^- anion [41]. According to these changes of Fe_3O_4:S after Pb(II) adsorption, it was demonstrated that the removal of Pb(II) was somehow owing to surface adsorption.

The Fe_3O_4:S NPs before and after Pb(II) adsorption were also analyzed by XPS. The survey scan XPS spectra were shown in Figure 10(a), the detected Pb species confirmed that Pb had been successfully adsorbed on the Fe_3O_4:S NPs. The high resolution spectrum of Pb 4f in Fe_3O_4:S NPs after adsorption shows two peaks, from which two distinct components can be resolved (Figure 10(b)). The peaks at 140.1 eV for Pb 4f 7/2 and 145.1 eV for Pb 4f 5/2 are assigned to Pb–O bonds [42]. And the binding energies of Pb 4f 7/2 at 138.8 eV and Pb 4f 5/2 at 143.8 eV are attributed to

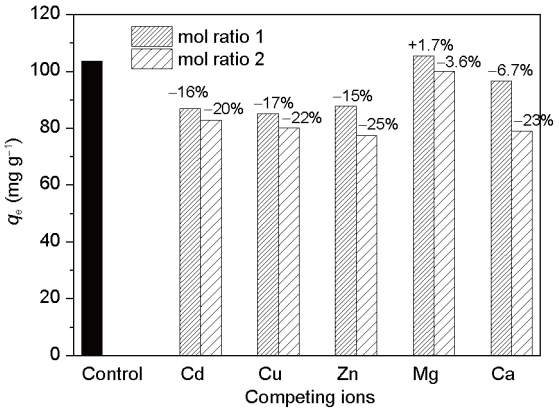

Figure 8 The effect of competing ions on the Pb(II) adsorption of Fe_3O_4:S NPs. Experimental conditions: initial Pb(II) concentration is 100 mg L^{-1} (50 mL), sorbent dosage is 30 mg, pH 6.0, contact time is 24 h, temperature is 30 °C.

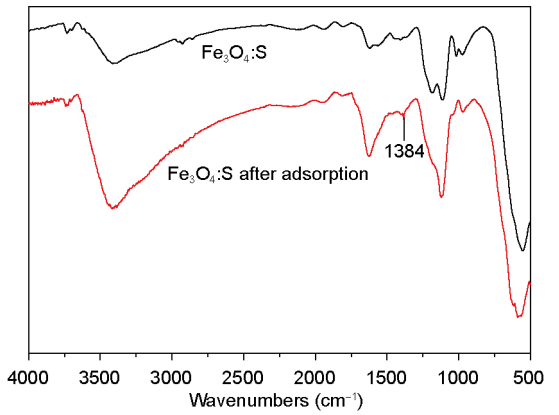

Figure 9 FTIR spectra of Fe_3O_4:S NPs before and after Pb(II) adsorption. Experimental conditions: initial Pb(II) concentration is 500 mg L^{-1}(80 mL), sorbent dosage is 60 mg, pH 6.0, contact time is 24 h, temperature is 30 °C (color online).

Pb in Pb–S [43,44]. It is further confirmed by the S 2p XPS spectrum (Figure 10(c)), the peaks at 164.0 and 165.3 eV of Fe_3O_4:S NPs after adsorption are ascribed to Pb–S [45,46]. The generation of PbS is a process of precipitation. The reaction is relatively fast due to the strong and selective soft-soft interactions between sulfur atoms and Pb(II) ions [47], and the lower solubility of PbS (K_{sp}=3.4×10^{-28}) could promote the sorption reaction between S and Pb^{2+}.

XRD spectra of Fe_3O_4:S NPs before and after adsorption with Pb(II) are depicted in Figure 11. It can be seen that there was almost no new peaks appeared after adsorption. Taken the XPS analysis results into consideration, this mainly owes to the fact that PbS existed in paracrystalline or amorphous form, or the amount of the crystals are not enough to detect.

Pb(II) ions undergo hydrolysis in aqueous solution [47]:

$$Pb^{2+} + mH_2O \leftrightarrow Pb(OH)_m^{(2-m)} + mH^+ \quad (5)$$

A higher pH would favor the adsorption of Pb(II) to a large extent, and electrostatic attraction might also be a key point

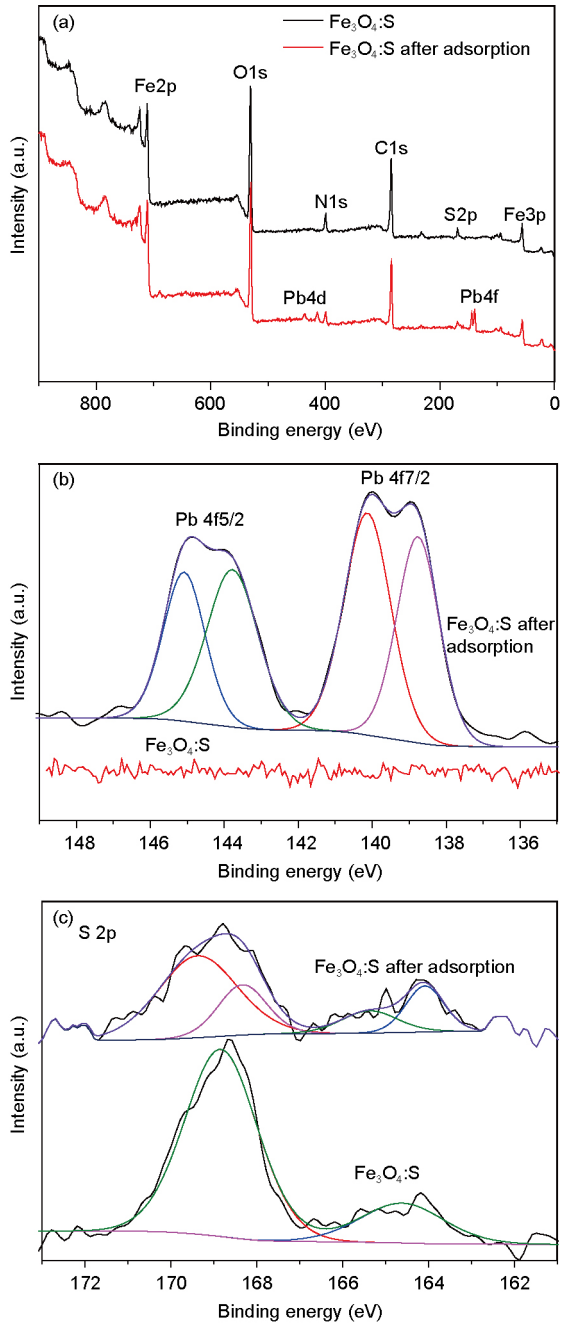

Figure 10 (a) Full-range XPS spectra of Fe_3O_4:S before and after Pb(II) adsorption; (b) Pb XPS spectra of Fe_3O_4:S before and after adsorption; (c) S XPS spectra of Fe_3O_4:S before and after adsorption. Adsorption experimental conditions were the same as above (color online).

to influence the adsorption capacity. As the pH of the solution increases, the number of negatively charged sites increases [48], and the specific surface area of the nano-adsorbent provides abundant adsorption sites for positively charged Pb(II) and $Pb(OH)_m^{(2n-m)}$.

On the basis of the analyses, it is rational to conclude that Pb(II) is removed from water due to a combination of precipitation, hydrolysis, and surface adsorption.

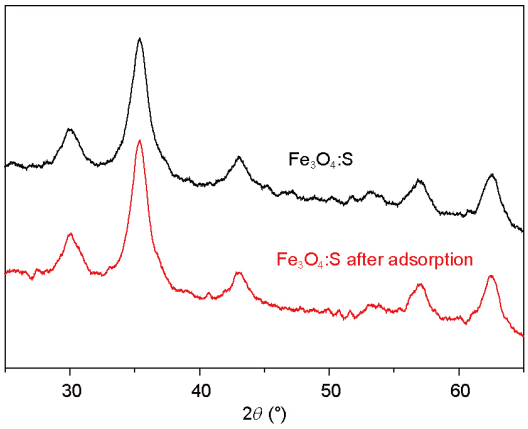

Figure 11 XRD spectra of Fe_3O_4:S NPs before and after Pb(II) adsorption. Adsorption experimental conditions were the same as above (color online).

4 Conclusions

In summary, Fe_3O_4:S NPs were synthesized with a novel simple strategy. After multicomponent mixing at low temperature and high temperature sintering, sulfur was successfully doped into Fe_3O_4 nanoparticles. Batch sorption studies showed that the Fe_3O_4:S NPs exhibited an efficient removal of Pb(II) in comparison with bare Fe_3O_4. The pseudo-second-order model provided a very good fitting (R^2=0.999) for Pb(II) adsorption. The Freundlich model was more favorable to present the Pb(II) adsorption process. The dominant mechanisms of Pb(II) removal were verified to be precipitation (formation of PbS), hydrolysis, and surface adsorption. Moreover, the adsorbent can be efficiently separated from the aqueous solution via an external magnetic field. Therefore, the Fe_3O_4:S NPs have great potential for Pb(II) removal from wastewater.

Acknowledgments This work was supported by the National Natural Science Foundation of China (B21271179, 21607101), Program for New Century Excellent Talents in University (NCET-13-0364), China Postdoctoral Science Foundation Funded Project (2016M590363), and State Key Program of National Natural Science Foundation of China (21436007).

Conflict of interest The authors declare that they have no conflict of interest.

1 Brebu M, Uddin MA, Muto A, Sakata Y, Vasile C. *Energy Fuels*, 2001, 15: 559–564
2 Frey NA, Peng S, Cheng K, Sun S. *Chem Soc Rev*, 2009, 38: 2532–2542
3 Gupta AK, Gupta M. *Biomaterials*, 2005, 26: 3995–4021
4 Laurent S, Forge D, Port M, Roch A, Robic C, Vander Elst L, Muller RN. *Chem Rev*, 2008, 108: 2064–2110
5 Shylesh S, Schünemann V, Thiel WR. *Angew Chem Int Ed*, 2010, 49: 3428–3459
6 Tang SCN, Lo IMC. *Water Res*, 2013, 47: 2613–2632
7 Tartaj P, Morales MP, González-Carreño T, Veintemillas-Verdaguer S, Serna CJ. *J Magn Magn Mater*, 2005, 290-291: 28–34

8 Sun HW, Zhang LY, Zhu XJ, Kong CY, Zhang CL, Yao SD. *Sci China Ser B-Chem*, 2009, 52: 69–75
9 Hua M, Zhang S, Pan B, Zhang W, Lv L, Zhang Q. *J Hazard Mater*, 2012, 211-212: 317–331
10 Periasamy K, Srinivasan K, Murugan PK. *Indian J Environ Health*, 1991, 33: 433–439
11 Wang L, Li J, Jiang Q, Zhao L. *Dalton Trans*, 2012, 41: 4544
12 Ji L, Zhou L, Bai X, Shao Y, Zhao G, Qu Y, Wang C, Li Y. *J Mater Chem*, 2012, 22: 15853
13 López KA, Piña MN, Quiñonero D, Ballester P, Morey J. *J Mater Chem A*, 2014, 2: 8796–8803
14 Liu Z, Wang H, Liu C, Jiang Y, Yu G, Mu X, Wang X. *Chem Commun*, 2012, 48: 7350–7352
15 Zhang C, Sui J, Li J, Tang Y, Cai W. *Chem Eng J*, 2012, 210: 45–52
16 Viltužnik B, Košak A, Zub YL, Lobnik A. *J Sol-Gel Sci Technol*, 2013, 68: 365–373
17 Yantasee W, Warner CL, Sangvanich T, Addleman RS, Carter TG, Wiacek RJ, Fryxell GE, Timchalk C, Warner MG. *Environ Sci Technol*, 2007, 41: 5114–5119
18 Wang M, Lei LP, Fang DH, Xu ZL, Chen SB. *J Agro-Environ Sci*, 2011, 30: 1669–1674
19 Wang Q. Synthesis of functionalized Fe_3O_4 nanoparticles for Hg(II) ions adsorption. *Dissertation for the Master's Degree*. Wuxi: Jiangnan University, 2012
20 Odio OF, Lartundo-Rojas L, Palacios EG, Martínez R, Reguera E. *Appl Surf Sci*, 2016, 386: 160–177
21 Thi TM, Trang NTH, Van Anh NT. *Appl Surf Sci*, 2015, 340: 166–172
22 Liang X, Zhu S, Zhong Y, Zhu J, Yuan P, He H, Zhang J. *Appl Catal B-Environ*, 2010, 97: 151–159
23 Liu R, Lu Y, Shen X, Yang X, Cui X, Gao Y. *J Nanosci Nanotech*, 2013, 13: 2835–2841
24 Rahimi R, Tadjarodi A, Rabbani M, Kerdari H, Imani M. *J Supercond Nov Magn*, 2013, 26: 219–228
25 Li L, Coates N, Moses D. *J Am Chem Soc*, 2010, 132: 22–23
26 Hwang SO, Kim CH, Myung Y, Park SH, Park J, Kim J, Han CS, Kim JY. *J Phys Chem C*, 2008, 112: 13911–13916
27 Patil AB, Patil KR, Pardeshi SK. *J Hazard Mater*, 2010, 183: 315–323
28 Raeisi Shahraki R, Ebrahimi M, Seyyed Ebrahimi SA, Masoudpanah SM. *J Magn Magn Mater*, 2012, 324: 3762–3765
29 Huberty JS, Madix RJ. *Surf Sci*, 1996, 360: 144–156
30 Chung TW, Yang J, Akaike T, Cho KY, Nah JW, Kim SI, Cho CS. *Biomaterials*, 2002, 23: 2827–2834
31 Kong L, Yan L, Qu Z, Yan N, Li L. *J Mater Chem A*, 2015, 3: 15755–15763
32 Ozverdi A, Erdem M. *J Hazard Mater*, 2006, 137: 626–632
33 Tang L, Feng H, Tang J, Zeng G, Deng Y, Wang J, Liu Y, Zhou Y. *Water Res*, 2017, 117: 175–186
34 Ling C, Liu FQ, Xu C, Chen TP, Li AM. *ACS Appl Mater Interf*, 2013, 5: 11808–11817
35 Ho YS, McKay G. *Proc Biochem*, 1999, 34: 451–465
36 Li Y, Du Q, Wang X, Zhang P, Wang D, Wang Z, Xia Y. *J Hazard Mater*, 2010, 183: 583–589
37 Dastkhoon M, Ghaedi M, Asfaram A, Goudarzi A, Langroodi SM, Tyagi I, Agarwal S, Gupta VK. *Separat Purif Tech*, 2015, 156: 780–788
38 Motsa MM, Mamba BB, Thwala JM, Msagati TAM. *J Colloid Interf Sci*, 2011, 359: 210–219
39 Li G, Zhao Z, Liu J, Jiang G. *J Hazard Mater*, 2011, 192: 277–283
40 Kim YJ, Kim MI, Yun CH, Chang JY, Park CR, Inagaki M. *J Colloid Interf Sci*, 2004, 274: 555–562
41 Ma L, Wang Q, Islam SM, Liu Y, Ma S, Kanatzidis MG. *J Am Chem Soc*, 2016, 138: 2858–2866
42 Bocanegra SA, Scelza OA, de Miguel SR. *Appl Catal A-Gen*, 2013, 468: 135–142
43 Yousefi R, Cheragizade M, Jamali-Sheini F, Mahmoudian MR, Saaédi A, Huang NM. *Chin Phys B*, 2014, 23: 108101
44 Cheraghizade M, Yousefi R, Jamali-Sheini F, Saáedi A, Ming Huang N. *Mater Sci Semicond Proc*, 2014, 21: 98–103
45 Goha SW, Buckleya AN, Lamba RN, Fan LJ, Yang YW. *ECS Trans*, 2006, 3: 107–119
46 Morino N, Kitagawa K, Morita T, Kimura S. *Thin Solid Films*, 2005, 479: 261–268
47 Ai K, Ruan C, Shen M, Lu L. *Adv Funct Mater*, 2016, 26: 5542–5549
48 Nassar NN. *J Hazard Mater*, 2010, 184: 538–546